Journal of Hazardous Materials 383 (2020) 121131

Contents lists available at ScienceDirect

Journal of Hazardous Materials

journal homepage: www.elsevier.com/locate/jhazmat

Variation in the mercury concentration and stable isotope composition of atmospheric total suspended particles in Beijing, China

Qiang Huang[a,*], John R. Reinfelder[b], Pingqing Fu[c], Weilin Huang[b]

[a] State Key Laboratory of Environmental Geochemistry, Institute of Geochemistry, Chinese Academy of Sciences, Guiyang, 550081, China
[b] Department of Environmental Sciences, Rutgers University, New Brunswick, NJ, 08901, USA
[c] Institute of Surface-Earth System Science, Tianjin University, Tianjin, 300072, China

ARTICLE INFO

Editor: Daniel C.W. Tsang

Keywords:
Mass-independent fractionation
APEC summit
Atmospheric particulate mercury
Photoreduction

ABSTRACT

We investigated the effect of the temporary ban of local industrial activities during the Asia-Pacific Economic Cooperation (APEC) summit (4th–14th Nov 2014) in Beijing, China on total suspended particulate mercury (Hg_{TSP}) concentrations and isotope compositions. We measured Hg concentrations and isotope ratios in 33 TSP samples from central Beijing, including 21 samples collected from Jun 2012 to Apr 2014, and 12 samples collected from 14th Oct–19th Nov 2014. Volumetric concentrations of both TSP and Hg_{TSP} during the APEC summit were a factor of 2 lower than during the pre-APEC period, indicating substantial reductions in total particulate matter and Hg_{TSP} as a result of emissions controls. However, mass-normalized concentrations and mercury isotope ratios of Hg_{TSP} did not vary significantly between samples collected before, during, or after the APEC summit. These results show that local emissions are important sources of particle bound mercury (PBM) in Beijing and that their control can be used to immediately lower the volumetric concentration of Hg_{TSP}. They also indicate that a similarly complex mixture of sources contributed to PBM in Beijing before and during emissions controls were put in place and that PBM concentrations in Beijing are primarily controlled by emissions and secondarily by photoreduction.

1. Introduction

Mercury (Hg) is a global pollutant, highly mobile in the environment and toxic to humans and wildlife even at low levels (Driscoll et al., 2013). Hg is emitted to the atmosphere through natural and anthropogenic processes and is present in the atmosphere as three operationally defined forms including gaseous elemental Hg (GEM), gaseous oxidized Hg (GOM) and atmospheric particle-bound Hg (PBM) (Selin, 2009). GEM is the predominant form of Hg in ambient air, is chemically most stable, and can be transported globally. GEM can be oxidized to soluble and short-lived GOM species that may adsorb to aerosols to form PBM (Horowitz et al., 2017), and it is a major form of atmospheric Hg dry deposition in Arctic area (Obrist et al., 2017). GOM and PBM are readily transferred back to the Earth's surface via wet (i.e., rain and snow fall) and dry deposition (Huang et al., 2016a; Siudek et al., 2016), thereby providing substrate to microbial Hg methylation in aquatic ecosystems (Amos et al., 2012). By definition, PBM is the Hg bound to airborne particulate matter (PM) such as dust, soot, and sea salt aerosols, and can be transported regionally in the atmosphere (Selin, 2009). Prior studies showed that PM samples collected from urban or industrial areas had much higher volumetric PBM concentrations (ng/m^3) than from rural areas, indicating significant anthropogenic contributions to PBM (Schleicher et al., 2015).

Anthropogenic activities in China are regarded as one of the largest atmospheric mercury emission sources even at the global scale (Zhang et al., 2015a; Fu et al., 2012; Streets et al., 2005), accounting for three-quarters of anthropogenic Hg emission from the East and Southeast Asia, or approximately one third of total global Hg emissions (AMPA, 2013). Fossil fuel combustion (mainly coal), nonferrous metal smelting, and cement production are the dominant sources of Hg to the atmosphere in China, collectively accounting for over 80% of total Hg emissions (Zhang et al., 2015a). PBM in urban environments of China is also emitted by multiple sources. Coal combustion for both heating and power generation is the largest source of PBM as coal is the dominant energy source in China. Non-ferrous metal smelting (especially Zn smelting), cement production, Hg mining, biofuel and biomass combustion as well as solid waste incineration are other important PBM sources (Zhang et al., 2015a; Fu et al., 2012; Wu et al., 2016). In the past decade, a few studies investigated spatial and temporal variations of PBM concentrations and their source apportionments for megacities

* Corresponding author.
E-mail address: huangqiang@vip.gyig.ac.cn (Q. Huang).

https://doi.org/10.1016/j.jhazmat.2019.121131
Received 27 February 2019; Received in revised form 30 August 2019; Accepted 31 August 2019
Available online 31 August 2019
0304-3894/

such as Beijing (0.57 ± 0.55 ng/m^3) (Schleicher et al., 2015), Shanghai (1.3 ± 0.15 ng/m^3) (Chen et al., 2016) and Nanjing (1.1 ± 0.57 ng/m^3) (Zhu et al., 2014). Their results showed that, compared to cities outside of China, PBM concentrations in these three megacities were a factor of 5 to 30 times higher (Schleicher et al., 2015; Chen et al., 2016; Zhu et al., 2014; Zhang et al., 2015b; Li et al., 2017).

To meet the goals of the national "Atmospheric Pollution Prevention and Control Action Plan" (Chinese State Council, 2013), the Chinese government has imposed emission controls to reduce PM levels. Emission control measures, for example shutting down or halting production from factories and power plants, or halting all construction activities, and limiting the number of vehicles on the roads were implemented at a regional scale to improve air quality for both the 2008 Beijing Olympic Games and the 2014 Asia-Pacific Economic Cooperation (APEC) summit. These events provided opportunities to study how emissions control measures affected air quality in Beijing and its surrounding areas. A number of previous studies reported much improved air quality during these emissions control events (Mo et al., 2018; Yu et al., 2018; Wang et al., 2010; Schleicher et al., 2016; Chen et al., 2015; Sun et al., 2016a). Wang et al. (2010) analyzed the daily emissions of major air pollutants during the 2008 Olympic Games in Beijing (8th–24th Aug, 2008) and found that the emissions of SO_2, NO_x, PM_{10}, and non-methane volatile organic compounds were, respectively, 41, 47, 55 and 57% lower than during the pre-control period of June 2008. Schleicher et al. (2016) found that volumetric concentrations (ng/m^3) of total suspended particle (TSP) bound mercury (Hg_{TSP}) were lower in Beijing in Aug 2008 (Olympic Games) than during the same month from 2006 to 2011, but no significant difference was found for mass-normalized Hg concentrations (ng/g) in the same TSP samples. Chen et al. (2015) found that the volumetric concentrations of aerosol species (organics, nitrate and sulfate) were 40–80% lower during than prior to the APEC summit. Similarly, Sun et al. (2016a) reported reductions in the concentrations of secondary inorganic aerosols (61–67% and 51–57%) and secondary organic aerosols (55% and 37%) at 260-m elevation and ground level, respectively, during the APEC meeting. The results of these studies show that regional-scale emissions controls substantially reduced both air pollutants and PM levels and suggest that meteorological conditions may play an important role in the observed variation of such reductions. They also suggest that further studies are needed to understand how mandatory emission controls affect the chemical composition, sources and formation mechanisms of PM under variable meteorological conditions.

The aim of the present study was to examine the responses of Hg_{TSP} and its mercury isotope composition to the implementation of emissions controls during the 2014 APEC summit, which was held on 5th–11th Nov in Beijing. Mercury stable isotopes have been used in recent studies to trace pollution sources and back-track transformations of Hg in the atmosphere (Chen et al., 2012; Sherman et al., 2012; Enrico et al., 2016). In this study, we collected 12 TSP samples from 14th Oct to 19th Nov 2014, including 3 samples during the emissions control period (3rd–12th Nov 2014), and 21 TSP samples from Jun 2012 to Apr 2014. We measured the Hg stable isotope compositions as well as the volumetric and mass-based concentrations of Hg of all TSP samples. The responses of TSP concentrations and both Hg_{TSP} concentrations and mercury isotope ratios to emissions controls were elucidated by quantifying differences in these values for pre-, during- and post-APEC summit periods, and were then compared to prior results from different emissions control events.

2. Methodology

2.1. Field site, sampling/method, and pre-concentration of Hg_{TSP}

The study site was located at the Institute of Atmospheric Physics, Chinese Academy of Sciences, between north 3rd and 4th ring road of Beijing. Detailed site information is available elsewhere (Huang et al., 2016b). Each atmospheric TSP sample was collected continuously over 71 h on a pre-combusted (450 °C for 4 h) quartz fiber filter (Pallflex 2500 QMT-UP, 20 × 25 cm^2, Pallflex Product Co., USA) using a high volume sampler at a steady flow rate of 1.0 m^3/min. Each sample represented a total volume of approximately 4000 m^3 of air over three consecutive days. A total of 33 samples were collected, 28 of which were collected in the pre-APEC summit period from Jun 2012 to Apr 2014 and 14th Oct to 4th Nov 2014, numbered Pre-1 to Pre-28, and 3 of which were collected during the APEC period from 4th to 14th Nov (emissions controls were implemented from 3rd to 12th Nov 2014), numbered as D-1 to D-3. An additional 2 samples were collected in the post-APEC period from 14th to 19th Nov, numbered as P-1 and P-2. A total of six field blanks were collected during two sampling campaigns and exposed to ambient conditions only for the length of time (< 15 min) required to set up the routine TSP samples. At the completion of each sampling event, filters were wrapped in aluminum foil, packed in plastic bags, and stored at −20 °C in the lab prior to analysis. The mass of TSP on each filter was measured gravimetrically by mass difference before and after sampling. Hg bound on each TSP sample was thermally extracted and concentrated for the analysis of Hg concentration and Hg stable isotopes following the procedures reported elsewhere (Huang et al., 2015). In brief, each filter sample was combusted stepwise in a dual-stage system and the combustion product was carried by Hg-free O_2 gas into a 5-mL acid-trapping solution (4 N HNO_3 and 1.5 N HCl). Acid-trapping solutions were transferred to 40-mL pre-cleaned (at 500 °C for 4 h) borosilicate glass bottles, diluted with 5-mL Milli-Q water and stored at 4 °C prior to Hg concentration and isotope measurements. The accuracy and precision of the sample treatment protocol were evaluated by the analysis of the certified reference material (CRM) GBW07405 following the same procedures. CRM GBW07405, a Yellow-Red Soil standard (National Center for Standard Materials, Beijing, China) with certified Hg concentration of 0.29 ± 0.03 μg/g, δ^{202}Hg value of −1.81 ± 0.15‰, and Δ^{199}Hg value of −0.34 ± 0.02‰, was used in previous studies (Huang et al., 2016b, 2015; Huang et al., 2019) for method development and evaluation. Meteorological data were obtained from China Meteorological Data Service Center (http://data.cma.cn/en, last access: 23rd June, 2016), arriving air mass directions were calculated using the US National Oceanic and Atmospheric Administration's (NOAA) backward HYSPLIT trajectory analysis (http://ready.arl.noaa.gov, last access: 2nd June, 2018), and both sets of data are listed in the Supporting Information Table S1.

2.2. Mercury content and its isotopic composition measurements

A small fraction (100 μL) of each pre-concentrated Hg solution was used to measure the total Hg content by cold-vapor atomic fluorescence spectroscopy (CVAFS, Tekran 2500, Tekran® Instruments Corporation, CA), with a precision of better than 10%. The analytical procedures used in this study were the same as reported previously (Huang et al., 2015). In brief, the 100-μL Hg solution was added to a 1% $SnCl_2$ solution to reduce Hg^{2+} to the Hg^0 form, which was purged from the solution using a Hg-free N_2 stream and collected on a gold-coated bead trap. Quantification of Hg was accomplished using a CVAFS analyzer. The amounts of detectable Hg in the field blank samples (< 0.2 ng, n = 6) were negligible (< 2%) compared to the amounts of total Hg (> 10 ng) in both the TSP samples and CRM GBW07405. The recoveries of Hg for CRM GBW07405 were in the acceptable range of 95 to 105%.

The Hg isotope compositions were analyzed using a multi-collector inductively coupled plasma mass spectrometer (MC-ICP-MS, Nu Instruments Ltd., UK) equipped with a continuous flow cold vapor generation system. The detailed protocols for Hg isotope analysis can be found elsewhere (Huang et al., 2015). Hg has seven stable isotopes (^{196}Hg, ^{198}Hg, ^{199}Hg, ^{200}Hg, ^{201}Hg, ^{202}Hg and ^{204}Hg), and two (^{196}Hg and ^{204}Hg) were not measured in this study due to their low natural abundances (0.15 and 6.82%, respectively). Instrumental mass bias was

corrected using an internal standard (NIST SRM 997 Tl) and strict sample-standard bracketing with NIST SRM 3133 Hg standard. Hg isotopes can undergo mass-dependent fractionation (MDF) during Hg transformation and transport processes (Bergquist and Blum, 2007; Sherman et al., 2010). Delta (δ) notation is used to represent MDF in units of per mil (‰) as defined in the following equation (Blum and Bergquist, 2007):

$$\delta^{x}\text{Hg}\ (‰) = [(^{x}\text{Hg}/^{198}\text{Hg})_{sample}/(^{x}\text{Hg}/^{198}\text{Hg})_{NIST3133} - 1] \times 1000 \quad (1)$$

where x = 199, 200, 201, or 202. Hg isotopes can also undergo mass-independent fractionation (MIF), which is reported as the deviation of a measured delta value from the theoretically predicted MDF value according to the equation:

$$\Delta^{x}\text{Hg}\ (‰) = \delta^{x}\text{Hg} - \beta \times \delta^{202}\text{Hg} \quad (2)$$

where the mass-dependent scaling factor β is about 0.252, 0.5024 and 0.752 for ^{199}Hg, ^{200}Hg and ^{201}Hg, respectively (Blum and Bergquist, 2007).

For quality assurance and quality control, a NIST SRM 3177 Hg standard was used as a secondary standard that was calibrated periodically against the NIST SRM 3133, and analyzed repeatedly during each analysis session. Measurements of the NIST 3177 standard yielded average δ^{202}Hg, Δ^{199}Hg and Δ^{201}Hg values of −0.53 ± 0.09‰, −0.01 ± 0.04‰ and −0.01 ± 0.07‰ (2SD, n = 17). A well-known reference material UM-Almaden and the CRM GBW07405 were also analyzed regularly for quality control, and the results showed average δ^{202}Hg, Δ^{199}Hg and Δ^{201}Hg values of −0.60 ± 0.09‰, −0.01 ± 0.04‰ and −0.03 ± 0.07‰ (2SD, n = 17) and of −1.77 ± 0.14‰, −0.29 ± 0.06‰ and −0.32 ± 0.07‰ (2SD, n = 6), respectively, consistent with the results of previously published studies (Huang et al., 2015; Blum and Bergquist, 2007). Uncertainties with respect to the measured isotope ratios of the 33 samples listed in Table 1 were calculated based on duplicate measurements.

3. Results and discussion

3.1. Response to emissions control

Both mass-based and volumetric concentrations are commonly used in atmospheric sciences as mass-based concentration is more appropriate for discussion of reaction processes and isotope fractionation whereas volumetric concentration is the unit used in the context of air quality and regulatory standards. In this study, we used both units where appropriate for discussion of mercury pollution in the context of processes and standards.

Variation of the volumetric concentrations of TSP and Hg_{TSP}, the mass-based concentrations of Hg_{TSP} and Hg isotope ratios (including δ^{202}Hg and Δ^{199}Hg) for the 33 TSP samples from pre-, during- and post-APEC periods are shown in Table 1. To clearly illustrate the response to emissions control, TSP concentrations, volumetric and mass-based Hg_{TSP} concentrations and Hg isotope compositions of 12 samples from 14th Oct to 19th Nov 2014 are also presented in Fig. 1. Average TSP concentrations were approximately a factor of 2 lower ($p < 0.05$) in the during- and post-APEC periods, compared to the pre-APEC period, which is similar to the trend for $PM_{2.5}$ during the same event (Sun et al., 2016a). The volumetric concentrations of Hg_{TSP} were significantly ($p < 0.05$) lower in the during-APEC than pre-APEC sampling periods (Table 1 and Fig. 1b), whereas such concentrations in the during- and post-APEC periods were not significantly different ($p > 0.05$). Given the small number of samples (n = 2) from the post-APEC period, and their variability, it is difficult to confirm whether Hg_{TSP} concentrations returned to pre-control levels during the seven days following the cessation of emissions controls. However, a previous study shown that the concentrations of $PM_{2.5}$ and $PM_{2.5}$-bound polycyclic aromatic hydrocarbons were returned to pre-control levels after the emissions controls for the 2014 APEC summit in Beijing (Yu et al., 2018).

In contrast to volumetric concentrations, average mass-normalized concentrations of Hg_{TSP} were not statistically different ($p > 0.05$) in samples from the pre-, during- and post-APEC periods. As shown in Table 1 (see also Fig. 1c), the ranges and mean values were similar in pre- (0.33 to 1.3 μg/g, mean of 0.80 ± 0.30 μg/g, n = 28), during- (0.43 to 1.1 μg/g, mean of 0.65 ± 0.36 μg/g, n = 3) and post- (0.61 to 1.2 μg/g, mean of 0.90 ± 0.41 μg/g, n = 2) APEC periods. Therefore, while emissions control measures did lead to a reduction in the average volumetric concentration of Hg_{TSP}, a direct result of lower TSP levels, the mass-normalized concentration of Hg_{TSP} was unchanged.

There was no significant ($p > 0.05$) difference between δ^{202}Hg and Δ^{199}Hg values in pre-, during- or post-APEC periods (Table 1 and Fig. 1d and e). The similarity of the Hg isotope compositions suggests that Hg_{TSP} likely had similar primary sources and/or had undergone similar processes in the atmosphere regardless of emissions control.

It is interesting to note that one sample, Pre-12 collected during 5th to 8th Feb, 2013, had a uniquely low Δ^{199}Hg value of −1.39‰, compared to the Δ^{199}Hg values for the other 32 TSP samples (−0.47‰ to 0.46‰). While any explanation of this anomalously low value is speculative without additional information, we suggest that two possible causes to consider are fireworks and/or mercury photoreduction processes at snow surfaces. Xu et al. (2019) suggested that the fireworks during the Chinese New Year celebration might have caused the most negative Δ^{199}Hg value (−1.1‰) in $PM_{2.5}$ from Beijing on 31st Jan, 2014. Alternatively, Sherman et al. (2010) showed that, due to photochemical reduction of mercury, the Δ^{199}Hg value of Arctic snow was as low as −5.08‰. Nevertheless, we treat this datum as an outliner in the following discussion of Hg isotope compositions due to its uniquely low, odd MIF signature.

Prior studies (Zhang et al., 2015a; Schleicher et al., 2016) demonstrated that fossil fuel combustion, non-ferrous metal, steel, and cement production, and waste incineration are the main contributors of PBM in Beijing, and that local meteorological conditions (i.e. precipitation) as well as seasonal factors (i.e. increased coal combustion for heating in winter) may have caused large variation in PBM concentrations. It is likely that these same factors may have caused the large variations in TSP concentrations and Hg concentrations and isotope compositions we report here. As shown in Table S1, no wet precipitation was observed in the during-APEC period, nor was there a significant difference ($p > 0.05$) in relative humidity between the pre- and during-APEC periods. As a result, it is unlikely that the observed decrease in the volumetric concentrations of both TSP and Hg resulted from wet precipitation. However, it is possible that the decreased concentrations may have been influenced by the direction of the arriving air masses from northwest in the during-APEC period as the areas northwest of Beijing are much less polluted compared to areas to the southwest (Huang et al., 2019). The lack of a change in mass-based concentrations of Hg_{TSP} and Hg isotope signatures during the implementation of emissions controls, which resulted in lower levels of atmospheric oxidants (Chen et al., 2015; Sun et al., 2016a), may indicate that photooxidation of Hg(0) is less important to PBM concentrations in Beijing than primary emissions and photoreduction. Regardless of meteorological or chemical conditions, this result suggests that regardless of the meteorological conditions, the sources of Hg emissions contributing to PBM in Beijing air included a similarly complex mixture of sources as was dominant before emissions controls were put in place.

To further examine the sources and transformations of Hg_{TSP}, a Pearson Correlation analysis of studied parameters was performed (Table S2). Excluding sample Pre-12, volumetric Hg concentrations were significantly ($p < 0.05$) correlated with TSP concentrations (r = 0.635), but the mass-normalized concentrations of Hg_{TSP} were not significantly (p = 0.146) correlated with TSP. The difference between volumetric and mass-normalized concentrations of Hg_{TSP} supports the conclusion that the reduction of volumetric Hg_{TSP} concentrations during the implementation of emissions control was likely attributable

Table 1
Averaged TSP concentrations, Hg_{TSP} volumetric concentrations, Hg_{TSP} mass-based contents and Hg isotope ratios are given below.

No.	TSP (μg/m^3)	Hg (ng/m^3)	Hg (μg/g)	δ^{202}Hg (‰) ± 2SD	Δ^{199}Hg (‰) ± 2SD	Δ^{201}Hg (‰) ± 2SD
Pre-APEC period, n = 28						
Pre-1	283	0.26	0.91	−1.27 ± 0.14	−0.06 ± 0.06	−0.10 ± 0.07
Pre-2	201	0.13	0.63	−0.86 ± 0.14	0.20 ± 0.06	0.13 ± 0.07
Pre-3	95	0.07	0.74	−1.06 ± 0.14	0.06 ± 0.06	0.00 ± 0.07
Pre-4	515	0.21	0.40	−1.01 ± 0.14	0.22 ± 0.06	0.11 ± 0.07
Pre-5	170	0.15	0.86	−1.14 ± 0.14	−0.10 ± 0.06	−0.12 ± 0.07
Pre-6	116	0.07	0.57	−1.11 ± 0.14	0.19 ± 0.06	0.18 ± 0.07
Pre-7	241	0.16	0.68	−0.97 ± 0.14	−0.16 ± 0.06	−0.24 ± 0.07
Pre-8	379	0.57	1.5	−1.06 ± 0.14	−0.05 ± 0.06	−0.05 ± 0.07
Pre-9	113	0.15	1.3	−1.04 ± 0.14	0.05 ± 0.06	−0.01 ± 0.07
Pre-10	214	0.18	0.85	−1.23 ± 0.14	−0.05 ± 0.06	−0.07 ± 0.07
Pre-11	262	0.34	1.3	−1.16 ± 0.14	−0.04 ± 0.06	−0.11 ± 0.07
Pre-12*	137	0.15	1.1	−0.88 ± 0.14	−1.39 ± 0.06	−1.41 ± 0.07
Pre-13	169	0.11	0.67	−1.39 ± 0.14	−0.15 ± 0.06	−0.15 ± 0.07
Pre-14	588	0.37	0.63	−1.09 ± 0.14	0.20 ± 0.06	0.11 ± 0.07
Pre-15	405	0.17	0.43	−1.24 ± 0.14	0.09 ± 0.06	0.07 ± 0.07
Pre-16	278	0.24	0.85	−0.89 ± 0.14	0.03 ± 0.06	0.08 ± 0.07
Pre-17	579	0.47	0.80	−0.89 ± 0.14	−0.04 ± 0.06	−0.16 ± 0.07
Pre-18	632	0.24	0.38	−0.77 ± 0.14	0.09 ± 0.06	−0.04 ± 0.07
Pre-19	513	0.37	0.73	−0.98 ± 0.14	−0.29 ± 0.06	−0.39 ± 0.07
Pre-20	368	0.23	0.62	−0.69 ± 0.14	−0.16 ± 0.06	−0.17 ± 0.07
Pre-21	147	0.10	0.68	−0.61 ± 0.14	0.03 ± 0.06	−0.01 ± 0.07
Pre-22	227	0.13	0.56	−1.11 ± 0.14	0.21 ± 0.06	0.14 ± 0.07
Pre-23	710	0.23	0.33	−0.85 ± 0.14	0.26 ± 0.06	0.15 ± 0.07
Pre-24	304	0.34	1.1	−0.99 ± 0.14	−0.14 ± 0.06	−0.14 ± 0.07
Pre-25	437	0.49	1.1	−0.73 ± 0.14	−0.47 ± 0.06	−0.61 ± 0.07
Pre-26	207	0.14	0.65	−1.11 ± 0.14	−0.03 ± 0.06	−0.01 ± 0.07
Pre-27	404	0.46	1.1	−0.92 ± 0.14	−0.41 ± 0.06	−0.42 ± 0.07
Pre-28	130	0.12	0.93	−0.89 ± 0.14	0.46 ± 0.06	0.41 ± 0.07
Average ± SD	315 ± 176	0.24 ± 0.14	0.80 ± 0.30	−1.01 ± 0.17	−0.05 ± 0.33	−0.10 ± 0.33
During-APEC period, n = 3						
D-1	175	0.08	0.45	−1.09 ± 0.14	−0.05 ± 0.06	−0.01 ± 0.07
D-2	157	0.17	1.1	−0.91 ± 0.14	0.09 ± 0.06	0.01 ± 0.07
D-3	189	0.08	0.43	−1.15 ± 0.14	0.26 ± 0.06	0.15 ± 0.07
Average ± SD	173 ± 16	0.11 ± 0.05	0.65 ± 0.36	−1.05 ± 0.12	0.10 ± 0.16	0.05 ± 0.09
Post-APEC period, n = 2						
P-1	197	0.23	1.2	−1.07 ± 0.14	−0.18 ± 0.06	−0.20 ± 0.07
P-2	153	0.09	0.61	−0.51 ± 0.14	0.07 ± 0.06	0.06 ± 0.07
Average ± SD	175 ± 31	0.16 ± 0.10	0.90 ± 0.41	−0.79 ± 0.40	−0.05 ± 0.17	−0.07 ± 0.18
Total, n = 33						
Range	95 to 710	0.07 to 0.57	0.33 to 1.5	−1.39 to −0.51	−1.39 to 0.46	−1.41 to 0.41
Average ± SD	294 ± 170	0.22 ± 0.13	0.80 ± 0.30	−1.00 ± 0.18	−0.04 ± 0.31	−0.09 ± 0.31

* Sample Pre-12 had visible snow on the filter.

to the substantial reduction of overall TSP levels, mass-based Hg_{TSP} concentrations remained at relatively constant levels, regardless of whether Hg was supplied by local or regional sources.

Meanwhile, δ^{202}Hg values of Hg_{TSP} were not significantly ($p > 0.05$) correlated with TSP concentration or either volumetric or mass-based Hg concentrations, and had poor correlations with both Δ^{199}Hg, and Δ^{201}Hg values. This lack of correlations indicates that the δ^{202}Hg values of specific sources or processes were obscured by the mixing of Hg from multiple sources and a variety of biogeochemical reactions which are known to produce MDF of different sign and with a wide range and often overlapping degrees of isotopic fractionation (Bergquist and Blum, 2007; Sherman et al., 2010; Yang and Sturgeon, 2009; Kritee et al., 2007; Estrade et al., 2009; Ghosh et al., 2013; Smith et al., 2015; Wiederhold et al., 2010; Janssen et al., 2016). The Δ^{199}Hg values were linearly correlated ($p < 0.01$) with the Δ^{201}Hg ratio, yielding a slope of 0.98 ± 0.05 ($r^2 = 0.938$, $n = 32$). This is consistent with prior findings showing that the slope of Δ^{199}Hg versus Δ^{201}Hg was approximately 1.1 for $Hg_{PM2.5}$ (Huang et al., 2016b), Hg_{TSP} (Xu et al., 2017) and Hg_{PM10} (Das et al., 2016). Prior studies have also shown that greater degrees of odd-MIF mainly occurred during photochemical reactions including photoreduction (Bergquist and Blum, 2007; Sherman et al., 2010; Zheng and Hintelmann, 2009, 2010a; Rose et al., 2015), photo-demethylation (Bergquist and Blum, 2007; Rose et al., 2015), and photo-oxidation (Sun et al., 2016b). Smaller, but measurable degrees of odd-MIF were also reported for nonphoto-chemical, abiotic reduction of Hg(II) (Zheng and Hintelmann, 2010b) and evaporation of Hg^0 (Estrade et al., 2009; Ghosh et al., 2013). The odd-MIF of Hg isotopes was observed during the photoreduction of inorganic Hg^{2+} with a Δ^{199}Hg/Δ^{201}Hg ratio of about 1.0 (Bergquist and Blum, 2007; Sherman et al., 2010; Zheng and Hintelmann, 2009, 2010a; Rose et al., 2015), while in other processes (photo-demethylation, photo-oxidation, non-photo-chemical abiotic reduction and evaporation) the Δ^{199}Hg/Δ^{201}Hg ratio was above 1.3 (Bergquist and Blum, 2007; Estrade et al., 2009; Ghosh et al., 2013; Rose et al., 2015; Zheng and Hintelmann, 2010b). Thus, with a Δ^{199}Hg/Δ^{201}Hg ratio of 0.98 ± 0.05 the Hg_{TSP} we collected in Beijing likely included the residual of prior photoreduction reactions. This is further supported by a statistically significant ($p < 0.01$) positive correlation between Δ^{199}Hg and average daily solar radiation. Such correlations were reported in previous studies (Huang et al., 2016b, 2019) and are consistent with the photoreduction of atmospheric particulate Hg^{2+}. In addition, the statistically significantly ($p < 0.05$) negative correlation between Δ^{199}Hg and mass-based concentrations of Hg_{TSP} shows that elevated positive values of Δ^{199}Hg were associated with low mass-based concentrations of Hg_{TSP}, as would be expected if Hg_{TSP} had undergone photoreduction. However, the odd-MIF results from this study may not be used to further quantify Hg photoreduction during the transport of TSP in the atmosphere or to trace the sources of TSP emissions.

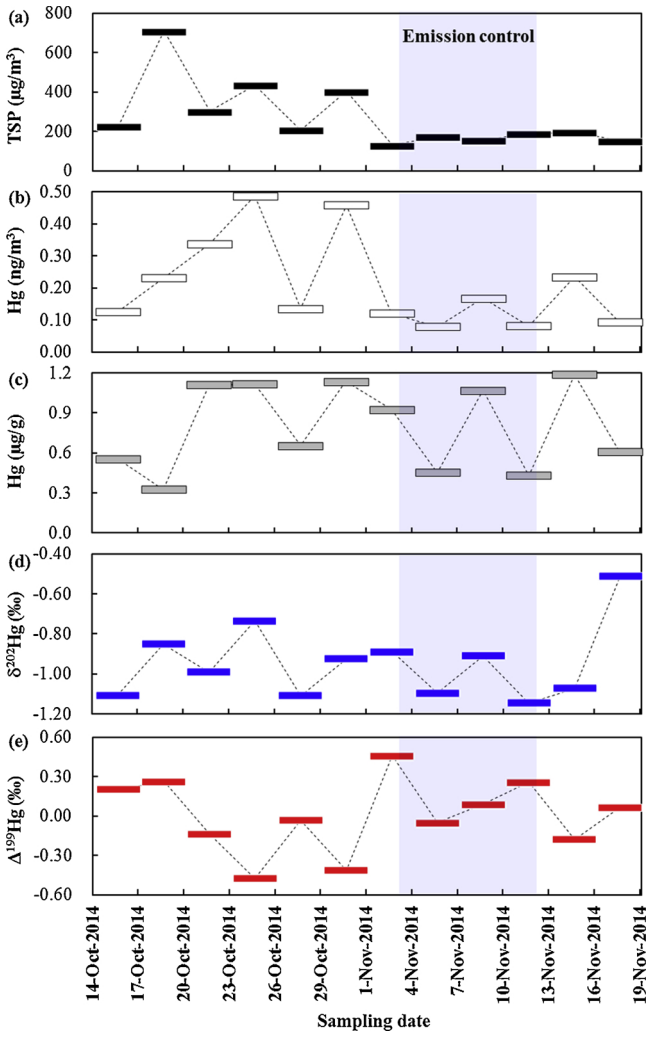

Fig. 1. Variation of TSP (a) and bound Hg (b and c) contents and Hg isotope ratios (d and e) for the TSP samples collected from 14th Oct to 19th Nov 2014. The shaded area shows the period of emission control during the APEC in Beijing.

3.2. Comparisons of the concentrations and Hg isotope compositions of PBM from major cities around the world

Mercury volumetric concentrations associated with aerosol particles of different size classes ($PM_{2.5}$, PM_{10} and TSP, respectively) from urban areas of different cities are listed in Table 2. The volumetric concentrations of Hg_{TSP} (mean of 0.22 ± 0.13 ng/m^3) in this study were comparable to those measured in Guiyang (0.25 ng/m^3) (Liu et al., 2011) and Qingdao (0.29 ng/m^3 during dust days and 0.19 ng/m^3 during non-dust days) (Zhang et al., 2015b), and were lower than in Xi'an (0.64 ± 0.54 ng/m^3) (Xu et al., 2017), Jinan (with $Hg_{PM2.5}$ mean of 0.51 ± 0.40 ng/m^3) (Li et al., 2017), Shanghai (0.56 ± 0.22 ng/m^3) (Xiu et al., 2009) and Nanjing (with Hg_{PM10} mean of 1.10 ± 0.57 ng/m^3) (Zhu et al., 2014). However, Hg_{TSP} concentrations observed in urban Beijing were still much higher than those measured in urban sites in developed countries, such as Poznan, Poland (0.02 ± 0.05 ng/m^3) (Siudek et al., 2016), Tokyo, Japan (with Hg_{PM10} mean of 0.10 ± 0.05 ng/m^3) (Sakata and Marumoto, 2002), and Birmingham, AL, USA (with average $Hg_{PM2.5}$ 0.04 ng/m^3) (Agnan et al., 2016).

As shown in Table 2, our data indicates that the volumetric concentrations of Hg_{TSP} in Beijing have been trending lower over the period of 2003 to 2014 (Schleicher et al., 2015, 2016; Wang et al., 2006). Previously reported average volumetric Hg_{TSP} concentrations form 2003 to 2006 were more than a factor of two higher than that from our study (0.22 ± 0.13 ng/m^3, n = 33). This dramatic decrease in Hg_{TSP} concentrations over a decade suggests that the control of particulate Hg emissions in Beijing and the surrounding regions of northeastern China has been very effective. Although the concentrations of Hg_{TSP} in the urban center of Beijing are still much higher compared to cities of many developed countries, the emissions control measures implemented during the APEC summit caused an immediate reduction of Hg_{TSP} by more than half.

Mercury isotope ratios for all TSP samples we collected except those for sample Pre-12 are comparable to the isotope compositions of $Hg_{PM2.5}$ measured in prior studies of $PM_{2.5}$ samples collected from the same site (Huang et al., 2016b, 2019). Specifically, the Hg isotope ratios of TSP samples (δ^{202}Hg from −1.39‰ to −0.51‰, mean of −1.00 ± 0.18‰, and Δ^{199}Hg from −0.47‰ to 0.46‰, mean of 0.00 ± 0.20‰, n = 32) overlapped those of the $PM_{2.5}$ samples (δ^{202}Hg from −2.18‰ to 0.55‰, mean of −0.58 ± 0.46‰, and Δ^{199}Hg from −0.53‰ to 1.04‰, means of 0.12 ± 0.32‰, n = 79) (Huang et al., 2016b, 2019). In addition, the isotope ratios of the Hg_{TSP} measured in this study were comparable to those of Hg_{TSP} from Xi'an (δ^{202}Hg from −1.45‰ to 0.08‰, mean of −0.80 ± 0.30‰, and Δ^{199}Hg from −0.34‰ to 0.25‰, mean of −0.02 ± 0.10‰, n = 67) (Xu et al., 2017) and Xiamen (δ^{202}Hg from −3.05‰ to 0.01‰, mean of −1.01 ± 0.79‰, and Δ^{199}Hg from −0.77‰ to 0.20‰, mean of −0.27 ± 0.20‰, n = 38) (Huang et al., 2018), China, but were higher than the δ^{202}Hg values reported for PM_{10} from urban areas of Kolkata, Eastern India (δ^{202}Hg from −3.48‰ to −0.12‰, mean of −1.64 ± 1.02‰, and Δ^{199}Hg values from −0.31‰ to 0.33‰, mean of −0.04 ± 0.17‰, n = 52) (Das et al., 2016), and were lower than Δ^{199}Hg values reported for TSP from the Grand Bay, MS, USA (with δ^{202}Hg from −1.61‰ to −0.12‰, mean of −0.87 ± 0.48‰, and with highly positive Δ^{199}Hg values from 0.36‰ to 1.36‰, mean of

Table 2
Comparison of PBM contents (in ng/m^3) in different cities.

City, Country	Time period	Size	Hg Concentration (ng/m^3)	Reference
Beijing, China	2003–2004	TSP	1.2 ± 0.8	(Wang et al., 2006)
	2006	TSP	0.57 ± 0.55	(Schleicher et al., 2015)
	08/2008 and 12/2008	TSP	0.23 ± 0.02 and 0.54 ± 0.24	(Schleicher et al., 2016)
	06/2012–11/2014	TSP	0.22 ± 0.13	This study
Guiyang, China	2009	TSP	0.25	(Liu et al., 2011)
Qingdao, China	2008–2011	TSP	dust day: 0.29, non-dust day: 0.19	(Zhang et al., 2015b)
Xi'an, China	11/2009–10/2012	TSP	0.64 ± 0.54	(Xu et al., 2017)
Jinan, China	2014–2015	$PM_{2.5}$	0.51 ± 0.40	(Li et al., 2017)
Shanghai, China	2004–2006	TSP	0.56 ± 0.22	(Xiu et al., 2009)
Nanjing, China	2011–2012	PM_{10}	1.10 ± 0.57	(Zhu et al., 2014)
Poznan, Poland	04/2013–10/2014	TSP	0.04 ± 0.05	(Siudek et al., 2016)
Tokyo, Japan	04/2000–03/2001	PM_{10}	0.10 ± 0.05	(Sakata and Marumoto, 2002)
Birmingham, AL, USA	2005–2008	$PM_{2.5}$	0.04	(Agnan et al., 2016)

0.83 ± 0.35‰, $n = 10$) (Rolison et al., 2013).

A prior study (Huang et al., 2016b) reported the Hg contents and isotope compositions of soil samples collected from parks and dust samples collected from road surfaces and rooftops near our sampling site in Beijing. While the mass-based concentration of Hg in TSP (0.81 ± 0.31 μg/g, $n = 28$) was significantly ($p < 0.05$) higher than that in the soil and dust samples (from 0.02 to 0.41 μg/g, mean of 0.15 μg/g, $n = 8$), δ^{202}Hg values in TSP (−1.39‰ to −0.51‰, −1.03 ± 0.18‰ 1SD, $n = 28$) were similar to those of the soil and dust samples (−1.14‰ to 0.35‰, mean of −0.74 ± 0.44‰), and the Δ^{199}Hg values of TSP samples (−0.47‰ to 0.46‰) overlapped with those of soil and dust samples (0.03‰ to 0.18‰, mean of 0.09 ± 0.04‰). This suggests that Hg_{TSP} may have contributed to the Hg in topsoil and dust of the urban area through direct dry deposition, and vice versa, but that the mercury isotope compositions remained unchanged after dry deposition or resuspension.

Novelty statement

This is the first report investigating the variations of TSP bound Hg (Hg_{TSP}) concentration as well as Hg stable isotope compositions during a strict temporary ban on local industrial activities. Our results show that such a temporary ban could immediately reduce the volumetric concentration of Hg_{TSP} resulting from reduced particulate emissions, but it may have limited impact on the mass-normalized concentration of Hg_{TSP} and its isotope compositions in urban air.

Acknowledgments

This study was supported financially by the National Key Research and Development Program of China (No. 2017YFC0212702), Natural Science Foundation of China (No. 41701268) and Guizhou Scientific Research Program (No. 20161158). The authors sincerely thank the anonymous reviewers for their constructive comments and suggestions. We also thank Dr. Jiubin Chen of Institute of Geochemistry, Chinese Academy of Sciences for his assistance during the initial phase of the study.

Appendix A. Supplementary data

Supplementary material related to this article can be found, in the online version, at doi:https://doi.org/10.1016/j.jhazmat.2019.121131.

References

Agnan, Y., Le Dantec, T., Moore, C.W., Edwards, G.C., Obrist, D., 2016. New constraints on terrestrial surface atmosphere fluxes of gaseous elemental mercury using a global database. Environ. Sci. Technol. 50, 507–524.

Technical Background Report for the Global Mercury Assessment 2013. Arctic Monitoring and Assessment Programme (AMAP) and United Nations Environment Programme (UNEP), Geneva, Switzerland.

Amos, H.M., Jacob, D.J., Holmes, C.D., Fisher, J.A., Wang, Q., Yantosca, R.M., Corbitt, E.S., Galarneau, E., Rutter, A.P., Gustin, M.S., Steffen, A., Schauer, J.J., Graydon, J.A., St Louis, V.L., Talbot, R.W., Edgerton, E.S., Zhang, Y., Sunderland, E.M., 2012. Gas-particle partitioning of atmospheric Hg(II) and its effect on global mercury deposition. Atmos. Chem. Phys. 12, 591–603.

Bergquist, B.A., Blum, J.D., 2007. Mass-dependent and -independent fractionation of Hg isotopes by photoreduction in aquatic systems. Science 318, 417–420.

Blum, J.D., Bergquist, B.A., 2007. Reporting of variations in the natural isotopic composition of mercury. Anal. Bioanal. Chem. 388, 353–359.

Chen, X., Balasubramanian, R., Zhu, Q., Behera, S.N., Bo, D., Huang, X., Xie, H., Cheng, J., 2016. Characteristics of atmospheric particulate mercury in size-fractionated particles during haze days in Shanghai. Atmos. Environ. 131, 400–408.

Chen, C., Sun, Y.L., Xu, W.Q., Du, W., Zhou, L.B., Han, T.T., Wang, Q.Q., Fu, P.Q., Wang, Z.F., Gao, Z.Q., Zhang, Q., Worsnop, D.R., 2015. Characteristics and sources of submicron aerosols above the urban canopy (260 m) in Beijing, China, during the 2014 APEC summit. Atmos. Chem. Phys. 15, 12879–12895.

Chen, J.B., Hintelmann, H., Feng, X.B., Dimock, B., 2012. Unusual fractionation of both odd and even mercury isotopes in precipitation from Peterborough, ON, Canada. Geochim. Cosmochim. Acta 90, 33–46.

Atmospheric pollution prevention and control action plan. Chinese State Council. (in Chinses, last access: 30 August 2019). http://www.gov.cn/zwgk/2013-09/12/content_2486773.htm.

Das, R., Wang, X., Khezri, B., Webster, R.D., Sikdar, P.K., Datta, S., 2016. Mercury isotopes of atmospheric particle bound mercury for source apportionment study in urban Kolkata, India. Elementa: Sci. Anthr. 4, 1–12.

Driscoll, C.T., Mason, R.P., Chan, H.M., Jacob, D.J., Pirrone, N., 2013. Mercury as a global pollutant: sources, pathways, and effects. Environ. Sci. Technol. 47, 4967–4983.

Enrico, M., Roux, G.L., Marusczak, N., Heimbürger, L.-E., Claustres, A., Fu, X., Sun, R., Sonke, J.E., 2016. Atmospheric mercury transfer to peat bogs dominated by gaseous elemental mercury dry deposition. Environ. Sci. Technol. 50, 2405–2412.

Estrade, N., Carignan, J., Sonke, J.E., Donard, O.F.X., 2009. Mercury isotope fractionation during liquid-vapor evaporation experiments. Geochim. Cosmochim. Acta 73, 2693–2711.

Fu, X.W., Feng, X.B., Sommar, J., Wang, S.F., 2012. A review of studies on atmospheric mercury in China. Sci. Total Environ. 421, 73–81.

Ghosh, S., Schauble, E.A., Lacrampe Couloume, G., Blum, J.D., Bergquist, B.A., 2013. Estimation of nuclear volume dependent fractionation of mercury isotopes in equilibrium liquid–vapor evaporation experiments. Chem. Geol. 336, 5–12.

Horowitz, H.M., Jacob, D.J., Zhang, Y.X., Dibble, T.S., Slemr, F., Amos, H.M., Schmidt, J.A., Corbitt, E.S., Marais, E.A., Sunderland, E.M., 2017. A new mechanism for atmospheric mercury redox chemistry: implications for the global mercury budget. Atmos. Chem. Phys. 17, 6353–6371.

Huang, Q., Liu, Y.L., Chen, J.B., Feng, X.B., Huang, W.L., Yuan, S.L., Cai, H.M., Fu, X.W., 2015. An improved dual-stage protocol to pre-concentrate mercury from airborne particles for precise isotopic measurement. J. Anal. At. Spectrom. 30, 957–966.

Huang, Q., Chen, J., Huang, W., Reinfelder, J.R., Fu, P., Yuan, S., Wang, Z., Yuan, W., Cai, H., Ren, H., Sun, Y., He, L., 2019. Diel variation in mercury stable isotope ratios records photoreduction of PM2.5-bound mercury. Atmos. Chem. Phys. 19, 315–325.

Huang, S., Sun, L., Zhou, T., Yuan, D., Du, B., Sun, X., 2018. Natural stable isotopic compositions of mercury in aerosols and wet precipitations around a coal-fired power plant in Xiamen, southeast China. Atmos. Environ. 173, 72–80.

Huang, J., Kang, S., Guo, J., Zhang, Q., Cong, Z., Sillanpää, M., Zhang, G., Sun, S., Tripathee, L., 2016a. Atmospheric particulate mercury in Lhasa city, Tibetan Plateau. Atmos. Environ. 142, 433–441.

Huang, Q., Chen, J., Huang, W., Fu, P., Guinot, B., Feng, X., Shang, L., Wang, Z., Wang, Z., Yuan, S., Cai, H., Wei, L., Yu, B., 2016b. Isotopic composition for source identification of mercury in atmospheric fine particles. Atmos. Chem. Phys. 16, 11773–11786.

Janssen, S.E., Schaefer, J.K., Barkay, T., Reinfelder, J.R., 2016. Fractionation of mercury stable isotopes during microbial methylmercury production by iron- and sulfate-reducing bacteria. Environ. Sci. Technol. 50, 8077–8083.

Kritee, K., Blum, J.D., Johnson, M.W., Bergquist, B.A., Barkay, T., 2007. Mercury stable isotope fractionation during reduction of Hg(II) to Hg(0) by mercury resistant microorganisms. Environ. Sci. Technol. 41, 1889–1895.

Li, Y., Wang, Y., Li, Y., Li, T., Mao, H., Talbot, R., Nie, X., Wu, C., Zhao, Y., Hou, C., Wang, G., Zhou, J., Qie, G., 2017. Characteristics and potential sources of atmospheric particulate mercury in Jinan, China. Sci. Total Environ. 574, 1424–1431.

Liu, N., Qiu, G.G., Landis, M.S., Feng, X.B., Fu, X.W., Shang, L.H., 2011. Atmospheric mercury species measured in Guiyang, Guizhou province, southwest China. Atmos. Res. 100, 93–102.

Mo, Y., Li, J., Jiang, B., Su, T., Geng, X., Liu, J., Jiang, H., Shen, C., Ding, P., Zhong, G., Cheng, Z., Liao, Y., Tian, C., Chen, Y., Zhang, G., 2018. Sources, compositions, and optical properties of humic-like substances in Beijing during the 2014 APEC summit: results from dual carbon isotope and Fourier-transform ion cyclotron resonance mass spectrometry analyses. Environ. Pollut. 239, 322–331.

Obrist, D., Agnan, Y., Jiskra, M., Olson, C.L., Colegrove, D.P., Hueber, J., Moore, C.W., Sonke, J.E., Helmig, D., 2017. Tundra uptake of atmospheric elemental mercury drives Arctic mercury pollution. Nature 547, 201–204.

Rolison, J.M., Landing, W.M., Luke, W., Cohen, M., Salters, V.J.M., 2013. Isotopic composition of species-specific atmospheric Hg in a coastal environment. Chem. Geol. 336, 37–49.

Rose, C.H., Ghosh, S., Blum, J.D., Bergquist, B.A., 2015. Effects of ultraviolet radiation on mercury isotope fractionation during photo-reduction for inorganic and organic mercury species. Chem. Geol. 405, 102–111.

Sakata, M., Marumoto, K., 2002. Formation of atmospheric particulate mercury in the Tokyo metropolitan area. Atmos. Environ. 36, 239–246.

Schleicher, N.J., Schäfer, J., Blanc, G., Chen, Y., Chai, F., Cen, K., Norra, S., 2015. Atmospheric particulate mercury in the megacity Beijing: spatio-temporal variations and source apportionment. Atmos. Environ. 109, 251–261.

Schleicher, N.J., Schafer, J., Chen, Y., Blanc, G., Chen, Y., Chai, F., Cen, K., Norra, S., 2016. Atmospheric particulate mercury in the megacity Beijing: efficiency of mitigation measures and assessment of health effects. Atmos. Environ. 124, 396–403.

Selin, N.E., 2009. Global biogeochemical cycling of mercury: a review. Annu. Rev. Environ. Resour. 34, 43–63.

Sherman, L.S., Blum, J.D., Keeler, G.J., Demers, J.D., Dvonch, J.T., 2012. Investigation of local mercury deposition from a coal-fired power plant using mercury isotopes. Environ. Sci. Technol. 46, 382–390.

Sherman, L.S., Blum, J.D., Johnson, K.P., Keeler, G.J., Barres, J.A., Douglas, T.A., 2010. Mass-independent fractionation of mercury isotopes in Arctic snow driven by sunlight. Nat. Geosci. 3, 173–177.

Siudek, P., Frankowski, M., Siepak, J., 2016. Atmospheric particulate mercury at the urban and forest sites in central Poland. Environ. Sci. Pollut. Res. 23, 2341–2352.

Smith, R.S., Wiederhold, J.G., Kretzschmar, R., 2015. Mercury isotope fractionation during precipitation of metacinnabar (β-HgS) and montroydite (HgO). Environ. Sci. Technol. 49, 4325–4334.

Streets, D.G., Hao, J., Wu, Y., Jiang, J., Chan, M., Tian, H., Feng, X., 2005. Anthropogenic mercury emissions in China. Atmos. Environ. 39, 7789–7806.

Sun, Y., Wang, Z., Wild, O., Xu, W., Chen, C., Fu, P., Du, W., Zhou, L., Zhang, Q., Han, T.,

Wang, Q., Pan, X., Zheng, H., Li, J., Guo, X., Liu, J., Worsnop, D.R., 2016a. "APEC blue": secondary aerosol reductions from emission controls in Beijing. Sci. Rep. 6, 20668.
Sun, G., Sommar, J., Feng, X., Lin, C.-J., Ge, M., Wang, W., Yin, R., Fu, X., Shang, L., 2016b. Mass-dependent and -independent fractionation of mercury isotope during gas-phase oxidation of elemental mercury vapor by atomic Cl and Br. Environ. Sci. Technol. 50, 9232–9241.
Wang, S., Zhao, M., Xing, J., Wu, Y., Zhou, Y., Lei, Y., He, K., Fu, L., Hao, J., 2010. Quantifying the air pollutants emission reduction during the 2008 Olympic Games in Beijing. Environ. Sci. Technol. 44, 2490–2496.
Wang, Z.W., Zhang, X.S., Chen, Z.S., Zhang, Y., 2006. Mercury concentrations in size-fractionated airborne particles at urban and suburban sites in Beijing, China. Atmos. Environ. 40, 2194–2201.
Wiederhold, J.G., Cramer, C.J., Daniel, K., Infante, I., Bourdon, B., Kretzschmar, R., 2010. Equilibrium mercury isotope fractionation between dissolved Hg(II) species and thiol-bound Hg. Environ. Sci. Technol. 44, 4191–4197.
Wu, Q., Wang, S., Li, G., Liang, S., Lin, C.-J., Wang, Y., Cai, S., Liu, K., Hao, J., 2016. Temporal trend and spatial distribution of speciated atmospheric mercury emissions in China during 1978–2014. Environ. Sci. Technol. 50, 13428–13435.
Xiu, G.L., Cai, J., Zhang, W.Y., Zhang, D.N., Bueler, A., Lee, S.C., Shen, Y., Xu, L.H., Huang, X.J., Zhang, P., 2009. Speciated mercury in size-fractionated particles in Shanghai ambient air. Atmos. Environ. 43, 3145–3154.
Xu, H.M., Sun, R.Y., Cao, J.J., Huang, R.-J., Guinot, B., Shen, Z.X., Jiskra, M., Li, C.X., Du, B.Y., He, C., Liu, S.X., Zhang, T., Sonke, J.E., 2019. Mercury stable isotope compositions of Chinese urban fine particulates in winter haze days: implications for Hg sources and transformations. Chem. Geol. 504, 267–275.
Xu, H., Sonke, J.E., Guinot, B., Fu, X., Sun, R., Lanzanova, A., Candaudap, F., Shen, Z., Cao, J., 2017. Seasonal and annual variations in atmospheric Hg and Pb isotopes in Xi'an, China. Environ. Sci. Technol. 51, 3759–3766.
Yang, L., Sturgeon, R., 2009. Isotopic fractionation of mercury induced by reduction and ethylation. Anal. Bioanal. Chem. 393, 377–385.
Yu, Q., Yang, W., Zhu, M., Gao, B., Li, S., Li, G., Fang, H., Zhou, H., Zhang, H., Wu, Z., Song, W., Tan, J., Zhang, Y., Bi, X., Chen, L., Wang, X., 2018. Ambient PM2.5-bound polycyclic aromatic hydrocarbons (PAHs) in rural Beijing: unabated with enhanced temporary emission control during the 2014 APEC summit and largely aggravated after the start of wintertime heating. Environ. Pollut. 238, 532–542.
Zhang, L., Wang, S.X., Wang, L., Wu, Y., Duan, L., Wu, Q.R., Wang, F.Y., Yang, M., Yang, H., Hao, J.M., Liu, X., 2015a. Updated emission inventories for speciated atmospheric mercury from anthropogenic sources in China. Environ. Sci. Technol. 49, 3185–3194.
Zhang, Y., Liu, R., Wang, Y., Cui, X., Qi, J., 2015b. Change characteristic of atmospheric particulate mercury during dust weather of spring in Qingdao, China. Atmos. Environ. 102, 376–383.
Zheng, W., Hintelmann, H., 2009. Mercury isotope fractionation during photoreduction in natural water is controlled by its Hg/DOC ratio. Geochim. Cosmochim. Acta 73, 6704–6715.
Zheng, W., Hintelmann, H., 2010a. Isotope fractionation of mercury during its photochemical reduction by low-molecular-weight organic compounds. J. Phys. Chem. A 114, 4246–4253.
Zheng, W., Hintelmann, H., 2010b. Nuclear field shift effect in isotope fractionation of mercury during abiotic reduction in the absence of light. J. Phys. Chem. A 114, 4238–4245.
Zhu, J., Wang, T., Talbot, R., Mao, H., Yang, X., Fu, C., Sun, J., Zhuang, B., Li, S., Han, Y., Xie, M., 2014. Characteristics of atmospheric mercury deposition and size-fractionated particulate mercury in urban Nanjing, China. Atmos. Chem. Phys. 14, 2233–2244.